Learning by Observation for Surgical Subtasks: Multilateral Cutting of 3D Viscoelastic and 2D Orthotropic Tissue Phantoms

Adithyavairavan Murali[1]*, Siddarth Sen[1]*, Ben Kehoe[2], Animesh Garg[3], Seth McFarland[2], Sachin Patil[1], W. Douglas Boyd[4], Susan Lim[5], Pieter Abbeel[1], Ken Goldberg[3]

***Abstract*— Automating repetitive surgical subtasks such as suturing, cutting and debridement can reduce surgeon fatigue and procedure times and facilitate supervised tele-surgery. Programming is difficult because human tissue is deformable and highly specular. Using the da Vinci Research Kit (DVRK) robotic surgical assistant, we explore a "Learning By Observation" (LBO) approach where we identify, segment, and parameterize sub-trajectories ("surgemes") and sensor conditions to build a finite state machine (FSM) for each subtask. The robot then executes the FSM repeatedly to tune parameters and if necessary update the FSM structure. We evaluate the approach on two surgical subtasks: debridement of 3D Viscoelastic Tissue Phantoms (3d-DVTP), in which small target fragments are removed from a 3D viscoelastic tissue phantom; and Pattern Cutting of 2D Orthotropic Tissue Phantoms (2d-PCOTP), a step in the standard Fundamentals of Laparoscopic Surgery training suite, in which a specified circular area must be cut from a sheet of orthotropic tissue phantom. We describe the approach and physical experiments, resulting in a success rate of 96% for 50 trials of the 3d-DVTP subtask and 70% for 20 trials of the 2d-PCOTP subtask. A video showcasing our LBO approach for multilateral cutting of 3D viscoelastic and 2D orthotropic tissue phantoms is available at: https://www.youtube.com/watch?v=beVWB6NtAaA.**

I. Introduction

Robotic surgical assistants (RSAs), such as Intuitive Surgical's da Vinci® system, have proven highly effective in facilitating precise minimally invasive surgery [10, 38]. Currently, these devices are primarily controlled by surgeons in a local tele-operation mode (master-slave with negligible time delays). Introducing autonomy of surgical subtasks has potential to assist surgeons, reduce fatigue, and facilitate supervised autonomy for remote tele-surgery.

Multilateral manipulation (with two or more arms) has potential to reduce the time required for surgical procedures, reducing the time patients are under anaesthesia and associated costs and contention for O.R. resources. Multilateral manipulation is also necessary for sub-tasks such as cutting and suturing; hand-off of tissue or tools between arms is common as each arm has limited dexterity and a workspace that may not cover the entire body cavity. Autonomous manipulation of deformable materials with two or more arms is of particular interest as surgical robot systems can be configured with three, four, or more arms.

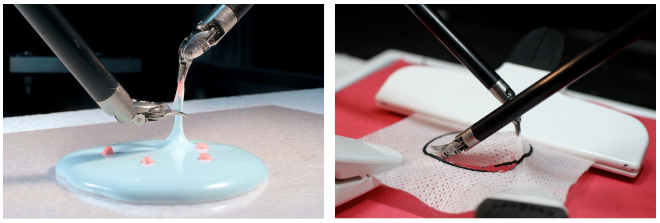

(a) (b)

Fig. 1: Autonomous multilateral surgical subtasks with the da Vinci Research Kit (DVRK). (a) Debridement of 3D Viscoelastic Tissue Phantoms (3d-DVTP) in which small target fragments are removed from a 3d-DVTP phantom. (b) Pattern Cutting of 2D Orthotropic Tissue Phantoms (2d-PCOTP) in which the objective is to cut out a specified circular area.

Automating manipulation and cutting presents challenges due to the difficulty of modeling the deformation behavior of highly nonlinear viscoelastic substances and the precision required for cutting. We apply a "Learning By Observation" (LBO) approach which involves observing human-operated demonstrations of a subtask and segmenting these demonstrations into motion sequences and transition conditions. In this work, we consider two surgical subtasks relevant to surgical procedures: debridement of viscoelastic tissue phantoms (3d-DVTP) and pattern cutting of orthotropic deformable tissue phantoms (2d-PCOTP). Surgical debridement is a tedious subtask in which dead or damaged tissue is removed from the body to allow the remaining healthy tissue to heal [14]. 2d-PCOTP is one of five subtasks in the commonly-used Fundamentals of Laparoscopic Surgery training suite. Surgical residents are trained to perform precision pattern cutting, and it is used to evaluate the performance of surgeons [12, 32].

We used the da Vinci Research Kit (DVRK) [16, 17] for our experiments. In our physical experiments, we achieved a success rate of 96% for 50 trials of the 3d-DVTP subtask and 70% for 20 trials of the 2d-PCOTP subtask.

II. Related Work

Robotic surgical systems have been used in a wide variety of surgical interventions [1, 5, 24, 35, 39]. In this work, we use the da Vinci Research Kit (DVRK) [16, 17], a research platform built from mechanical components from the first-generation of the da Vinci surgical system [4] and electronics and software from WPI and Johns Hopkins University. Padoy et al. [29] demonstrated execution of a human-

*The two first authors contributed equally to this work.
[1]Department of Electrical Engineering and Computer Science (EECS). {adithya_murali, siddarthsen, sachinpatil, pabbeel}@berkeley.edu
[2]Mechanical Engineering; {benk@berkeley.edu, mcf.seth@gmail.com}
[3]IEOR and EECS; {animesh.garg, goldberg}@berkeley.edu
[1–3] Center for Automation and Learning for Medical Robotics (Cal-MR); University of California, Berkeley; Berkeley, CA 94720, USA
[4]Division of Cardiothoracic Surgery; University of California Davis Medical Center; Sacramento, CA 95817, USA; walter.boyd@ucdmc.ucdavis.edu
[5]Centre for Breast Screening and Surgery, Centre for Robotic Surgery, Singapore; susanlim@berkeley.edu

Fig. 2: Debridement of a 3D Viscoelastic Tissue Phantom (3d-DVTP) with a linear tumor target. This subtask consists of five surgemes: motion, penetration, grasping, retraction, and cutting. Multiple debridement operations are needed to remove a single target.

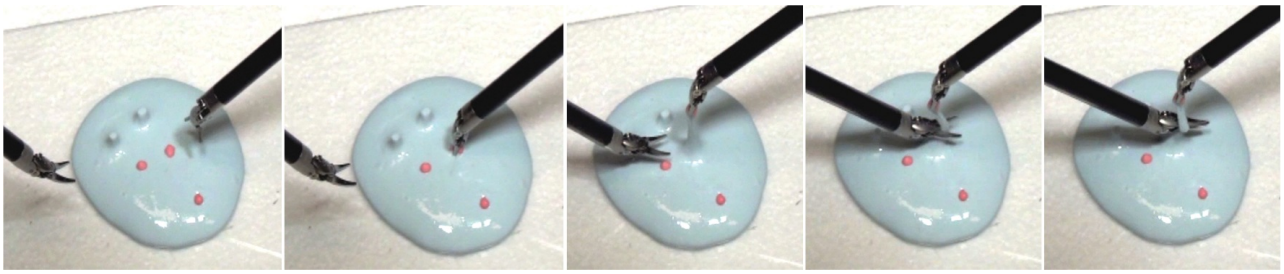

Fig. 3: Debridement of a 3D Viscoelastic Tissue Phantom (3d-DVTP) with spherical tumor targets. This subtask consists of five surgemes: motion, penetration, grasping, retraction, and cutting. The same finite state machine is used as in Figure 2.

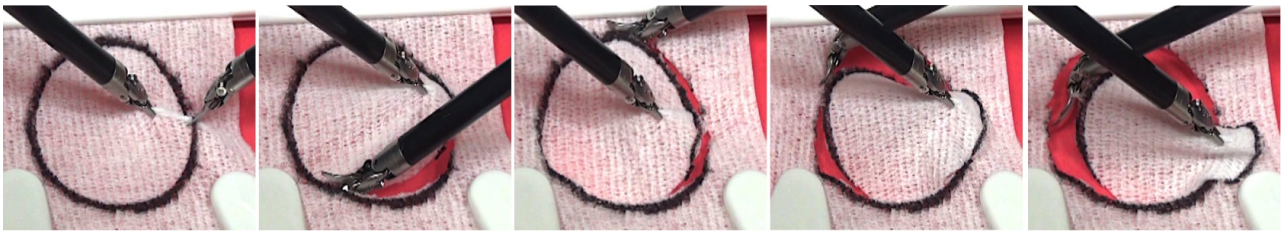

Fig. 4: Pattern Cutting of a 2D Orthotropic Tissue Phantom (2d-PCOTP). The finite state machine includes the following states: circle detection and estimation, warping, grasp OTP (push, grasp, retract), notch cutting (push, close, retract, twist), lower semicircle positioning, lower semicircle cutting, upper semicircle repositioning, upper semicircle cutting, active sensing for attachment detection (pull), and final cutting.

robot collaborative suturing task on the DVRK platform. The DVRK platform is being used in 16 research labs for tasks ranging from tissue palpation using an ultrasound probe for tumor detection [6] to autonomous tool tracking in ultrasound images [23]. We consider debridement of viscoelastic tissue phantoms, which extends our previous work in autonomous debridement [18] with the Raven surgical robot [15], an open-architecture research platform similar to the DVRK.

Manipulation of deformable materials, particularly cutting, is an area of research interest in robotic surgery [26] and in computer graphics and computational geometry [9, 40]. However, high fidelity models of viscoelastic tissue deformations are computationally expensive due to the need for re-meshing and finite element simulations.

Prior work has explored the use of expert demonstrations to handle deformations in environment without explicit models and simulations. Reiley et al. [31] proposed a demonstration-based framework that used Gaussian Mixture Models (GMMs) for motion generation. Van den Berg et al. [36] proposed an iterative technique to learn a reference trajectory and execute it at higher than demonstration speeds for suture knot tying. This work was recently extended by Osa et al. [28] to deal with dynamic changes in the environment, but with an industrial manipulator. Mayer et al. [22] use principles of fluid dynamics and Schulman et al. [33] use non-rigid registration techniques to generalize human demonstrations to similar, yet previously unseen, initial conditions. These approaches are broadly classified under the category of Learning From Demonstrations (LfD) [2, 8], where demonstration trajectories are directly modified for generalizing to test situations.

Segmentation of demonstrations into meaningful motion sequences has been extensively studied [13, 19, 25]. In the context of surgery, Hager et al. propose a "Language of Surgery" with "surgemes" analogous to phonemes [21, 30, 37]. Manual segmentation of surgemes in demonstrations have been used for understanding and recognizing surgical skills and subtasks, and for evaluating surgeon skills [30, 37].

III. Subtasks for Case Study

A. Debridement of 3D Viscoelastic Tissue Phantoms (3d-DVTP)

Surgical debridement is a tedious surgical subtask in which dead or damaged tissue is removed from the body to allow the remaining healthy tissue to heal faster [3, 14]. As shown in Fig. 2 and 3, we introduce an extension to the debridement task presented in our previous work [18].

We use a viscoelastic tissue phantom made from a mixture of Elmer's Glue, borax, and water. Embedded in the phantom are multiple targets of viscoelastic material of a tougher consistency. These targets represent damaged or tumorous tissue that must be removed from the surrounding phantom.

Autonomous surgical debridement of viscoelastic tissue requires perception to locate damaged tissue, grasp and motion planning to determine collision free trajectories for one or more arms and grippers to grasp them, and careful coordination of arms to retract and separate the damaged tissue from the VTP.

In this work, we consider targets that form convex regions, and in particular regions that, after any debridement operation, the targets left still form one or more convex regions. The maximum width of target material that can be removed in one debridement operation is d_w. We consider two types of convex regions: spherical regions of diameter $< d_w$, and linear regions of width $< d_w$.

B. Pattern Cutting of 2D Orthotropic Tissue Phantom (2d-PCOTP)

The second subtask, 2d-PCOTP, is shown in Figure 4. The Fundamentals of Laparoscopic Surgery (FLS) is a standard training regimen for medical students in laparoscopic surgery and consists of a suite of five subtasks of increasing complexity [32]. The second subtask in this suite is called "Pattern Cutting". This subtask features a 50 mm diameter, 2 mm thick circular pattern marked on a 4×4 inch square of surgical gauze suspended by clips. We assume that the circle lies in the horizontal plane. The subtask is complete once the circle has been cut from the surrounding gauze.

Metric: The FLS suite states that deviations under 2 mm from the line are not penalized. We define an inner circle, C_I, and an outer circle, C_O, at 2 mm inside and outside the pattern, respectively. We define the error E_I as the sum of the areas between C_I and the cut line falling inside C_I, and the error E_O as the area between C_O and the cut line falling outside C_O. With A the area of the annulus (Area of C_O-Area of C_I), we define the quality score as:

$$Q = 100\Big[1 - \frac{E_I + E_O}{A}\Big]. \tag{1}$$

This quality corresponds to the symmetric difference of the cut and the circle (as a percentage).

IV. System Architecture

A. da Vinci Research Kit (DVRK)

The da Vinci Research Kit (DVRK) is a development platform provided by Intuitive Surgical to advance research in teleoperated robotic surgical systems. It consists of proprietary hardware from the first-generation da Vinci "classic", and open-source electronics and software developed by WPI and Johns Hopkins University [17]. The robot hardware consists of two robotic laparoscopic arms, termed "Patient-Side Manipulators" (PSMs), and the Surgeon Console for teleoperating with a stereo viewer, two master controllers, termed "Master Tool Manipulators" (MTMs), and a set of foot pedals. The PSMs have interchangeable tools. We use two tools: the Large Needle Driver and the Curved Scissors. The Large Needle Driver is a grasper with 6 mm fingers. The Curved Scissors is a cutting instrument 10 mm in length. The PSM manipulates the attached instruments about a fixed point called the remote center of motion. The PSMs each have 6 degrees of freedom plus a grasp degree of freedom.

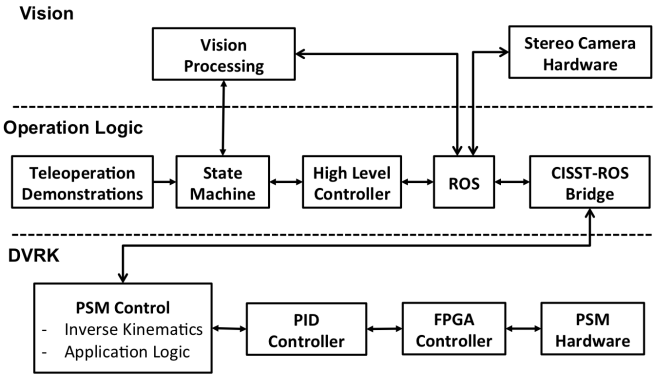

Fig. 5: Software Architecture. The software consists of three components: vision, operation logic, and the DVRK system software [17].

B. System Software

Software to control the da Vinci hardware is provided for the DVRK by JHU with their cisst/SAW libraries. This component-based framework provides DVRK-specific components to communicate with the electronics, along with generic components to enable PID control, teleoperation, recording, GUI development, and integration with ROS [17]. The high level architecture for our system is shown in Figure 5. We use the inverse kinematics and PID controllers from the DVRK system software. This allows us to control the robot using pose commands, working directly in Cartesian space instead of directly commanding motor torques.

C. Vision System

Due to tissue and tool specularity, perception using RGBD sensing is not feasible. We use two fixed stereo camera pairs, each composed of two Prosilica GigE GC1290C cameras with 6 mm focal length lenses. We use HSV (Hue, Saturation, Value) separation to classify different materials in the environment. We use a click interface to manually select pixels of each material in view of the camera. For each of the materials, we find a range of HSV values that contains all of its pixels, while excluding the HSV values of pixels from other materials. We perform this process when there is a change in the material properties or lighting conditions. We use the open-source OpenCV library [7].

V. Learning By Observation

We use a Learning By Observation (LBO) approach [11] for automation of surgical subtask execution. Figure 6 shows a schematic of our approach and the individual steps involved in the process are explained below:

1) Perform Task (Teleoperation): First, a domain expert performs a demonstration of the surgical subtask via teleoperation. We record motion of the MTMs and PSMs in terms of joint angle data from the encoders. For each demonstration, we also record sensor data consisting of images from the stereo camera pair.

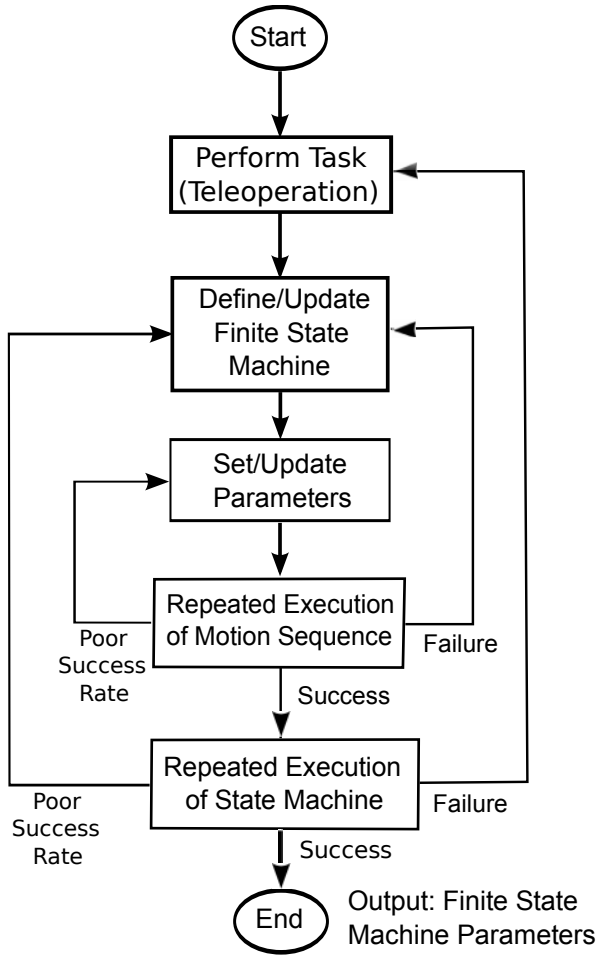

Fig. 6: The Learning By Observation process. A domain expert performs a demonstration task via teleoperation. We observe the demonstration and segment it into motion sequences and transition conditions, which is used to construct a finite state machine. Task specific parameters are defined and updated based on the success rate from repeated executions of motion sequences. The finite state machine is refined or new demonstrations are collected if the motion sequences cannot be successfully executed autonomously.

2) Define/Update Finite State Machine: We extract motion sequences and transition conditions from the collected demonstration data. In contrast to the unsupervised learning used by Dixon for segmentation of demonstrations, we consider a supervised learning approach in which the demonstrations are manually segmented into motion sequences.

We define important transition points as regions of the state space at a specific time point where change points occur; defining a change point as a time when the robot significantly changes its motion or initiates an interaction with the environment. For instance, the 3d-DVTP task consists of five motion sequences: motion, penetration, grasping, retraction, and cutting. The segmentation of a human demonstration into these sequences is based on motion cues such as change in velocity/accelerations or change in the contact with the gripper. In the 2d-PCOTP task, the motion sequences such as grasping, cutting a notch, and cutting lower and upper halves of the circle are similarly segmented.

3) Set/Update Parameters: Autonomous execution of each motion sequence in the finite state machine requires the definition of parameters. For instance, the 3d-DVTP retraction motion sequence requires a parameter value that specifies how high the target material is retracted after it is grasped. If this value is too low (lower bound: 1.5 cm), there is insufficient clearance for the scissors to move under the other gripper for accomplishing the cut. On the other hand, if the value is too high (upper bound: 7 cm), the retraction height approaches the remote center of motion, which is an upper bound on the motion of the manipulators. We empirically determine these bounds based on execution of each motion sequence and use binary search to determine the parameter value. For the retraction sequence, we used binary search to determine a value of 3 cm for our experiments. These parameters are also updated during the refinement of the finite state machine if required.

4) Repeated Execution of Motion Sequence: Each motion sequence is executed repeatedly to evaluate robustness during autonomous execution trials. We use the success rate over execution of 10 trials of each motion sequence. If the success rate is less than 75%, we update the parameters associated with the motion sequence execution using binary search and repeat the process. However, in certain situations, execution of the motion sequence fails most of the time with a success rate of less than 10%. For instance, the 2d-PCOTP task involves cutting a notch in the gauze for initiating the pattern cutting. However, the notch cutting motion sequence involves grasping the gauze and cutting but this sequence has a poor success rate of less than 10% during the repeated execution. In this case, we refine the finite state machine by separating the grasping and cutting sequences. In our experiments, we found this strategy to have a higher success rate. Once the desired success rate is achieved, we finalize the motion sequence and proceed to the next step.

5) Repeated Execution of State Machine: We test the repeatability of the state machine under multiple executions in terms of the success rate. If the success rate is less than 50%, we update the state machine. For instance, we augmented the 2d-PCOTP state machine with motion sequences to reposition the scissors into the notch in between cutting motions to improve the success rate. We also collect new demonstrations if the success rate is very low. In the 2d-PCOTP task, an initial demonstration cut the entire circular pattern in an anticlockwise direction but this motion sequence had a very low success rate. In our experiments, we found that separating the cutting motion into two separate motion sequences: cutting the lower and upper halves of the circle improves the success rate considerably. We finalize the finite state machine when a success rate of greater than 50% is achieved in 10 repeated trials.

We describe the application of our LBO approach to the two subtasks below.

A. Debridement of 3D Viscoelastic Tissue Phantom (3d-DVTP)

1) Perception: In the 3d-DVTP subtask, we first find the 3D centroids of the targets. To do this, we find the 2D centroids of each target in each of the left and right stereo

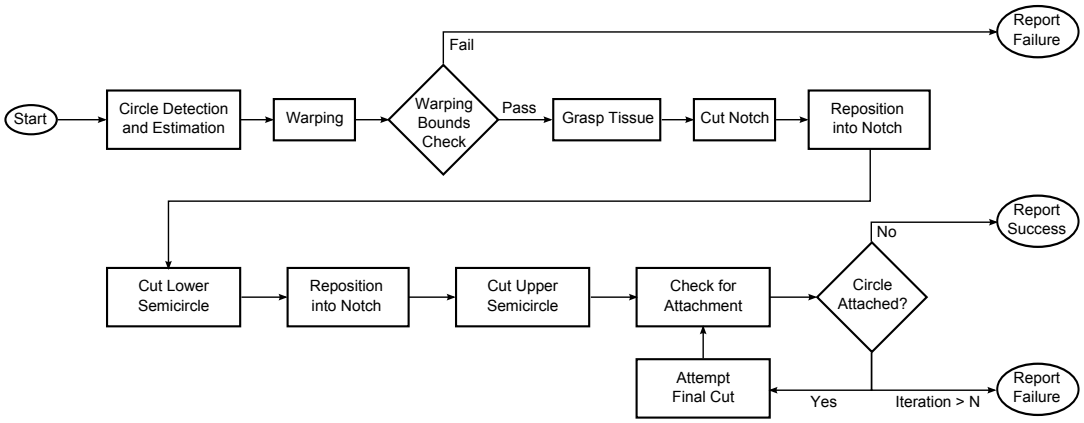

Fig. 7: Finite State Machine for 2d-PCOTP. This subtask includes ten states: circle detection and estimation, warping, grasp tissue (push, grasp, retract motions), notch cutting (involves push, close, retract, twist motions), lower semicircle positioning, lower semicircle cutting, upper semicircle repositioning, upper semicircle cutting, active sensing for attachment detection (pull), and final cutting.

images. For each image, we use HSV separation to find the pixels corresponding to the VTP. We use this as a bounding box to find the pixels of targets. We use OpenCV to find the contours among the target pixels.For each contour in each of the two stereo images, we find the centroid. We take the left-most centroid in the left image and find the corresponding centroid in the right image based on a sliding window. The resulting disparity gives the 3D centroid. We repeat this procedure until all matching centroids have been found. If no matching centroids are found, we consider the subtask to be complete, unless no targets have been debrided, in which case we consider the subtask to have failed. There is one parameter $p_1 = 100$ pixels which indicates the tolerance for finding contours among the target pixels.

2) Finite State Machine: We segmented the debridement demonstrations into five motion sequences based on when the robot significantly changes its motion or when the contact state with the gripper changes: approach, penetration, grasping, retraction, and cutting, with an associated parameter vector $p = (p_2, \ldots, p_7)$.

The approach sequence consists of moving the gripper to a point $p_2 = 1.2$ cm directly above the target. This is determined by a binary search between two empirically determined bounds—0.5 cm and 5 cm. The penetration sequence moves vertically down until the tips of the gripper fingers are approximately $p_3 = 4$ mm into the tissue, which is also a lower bound on the penetration distance for successful grasping and extraction of the target. The grasping sequence is the closure of the gripper on the target without movement. The retraction sequence pulls the target and surrounding material $p_4 = 3$ cm vertically. The retraction distance is determined by using binary search between the lower bound of 1.5 cm and upper bound of 7 cm. In the cutting sequence, the cutting tool moves until the tips of the cutting tool are $p_5 = 4$ mm past the center of the retracted material (the length of the scissor gripper is 10 mm), $p_6 = 2.8$ cm below the gripper and then the scissors are closed. For the retraction surgeme, the gripper moves at a speed of $p_7 = 0.5$ cm/s. This value was determined by using a binary search between empirical bounds of 0 cm/s and upper bound of 5 cm/s, beyond which the material snaps during retraction.

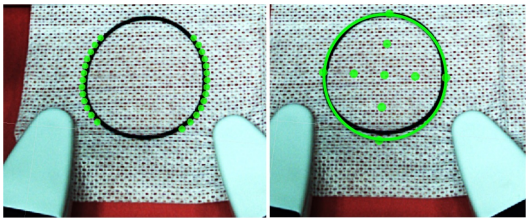

Fig. 8: Estimation of elliptical pattern on the Orthotropic Tissue Phantom in the 2d-PCOTP subtask. We use HSV thresholding to find a contour of the pattern outline. Then, stereo matching is performed to estimate the 3D location of points along the left and right quadrants of the circle. Finally, using the set of 3D points on the pattern boundary, an ellipse is fit to these 3D points using least-squares.

B. Pattern Cutting of 2D Orthotropic Tissue Phantom (2d-PCOTP)

Using the LBO approach, we construct a finite state machine for the 2d-PCOTP task as shown in Figure 7. Each state may execute multiple sequences, and may have one or more parameters. We identified ten states, two sensor conditions, and thirteen motion sequences.

For our experiments, we varied the position of the center of the circle to evaluate the effectiveness of the finite state machine. We manually set bounds on the translation to ensure safety of the resulting trajectories. Due to the close proximity of the OTP fixture clips as shown in Figure 1(b), translation in the y direction was limited to 5 mm.

1) Circle Detection and Estimation: The first state involves finding the 3D position of the circle pattern. We find the outer contour of the circle using thresholding, similar to the one in Section V-A. To find 3D points that we can use for ellipse fitting from the contour of the image, we find correspondences between the contours in the left and right stereo images. We use least squares to fit an ellipse to the points in the plane (see Figure 8b).

2) Translation: In this step, we find a rigid translation between the circle pattern detected for the demonstration and the current circle pattern as detected in the previous state. This allows us to translate the recorded motion sequences to the new environment.

3) Grasp Tissue: The third state has the purpose of pulling the OTP taut to allow the cutting tool to make an incision. We observed three motion sequences in the demonstration. First, the open gripper pushes the material down until it contacts the surface below. Then, the gripper closes, folding and grasping a section of the OTP. Finally, the gripper lifts vertically to pull the OTP taut. This forms a ridge, which the cutting tool takes advantage of to cut a notch in the material, as can be seen in Figure 4a.

4) Cut Notch: The fourth state is the most complicated of the demonstration trajectories. The FLS rules allow a surgeon to either cut a notch to begin the subtask or to cut in from the edge. We observed a cycle of surgemes in the demonstration. First, with the cutting tool open, the tool pushes down on the OTP. Second, the cutting tool closes. Third, the cutting tool retracts. This process is repeated three times to ensure a higher success rate across repeated executions of the sequence.

5) Reposition into Notch for Lower Semicircle: The fifth state uses a single motion sequence. We observed that this trajectory approached the notch along the line that it would start cutting.

6) Cut Lower Semicircle: The sixth state uses a single motion sequence. The sequence cuts along the lower arc of the pattern approximately halfway around.

7) Reposition into Notch for Upper Semicircle: The seventh state uses a single motion sequence. Similar to the earlier repositioning, the demonstration trajectory slowly approached the point to be cut along the line of cutting.

8) Cut Upper Semicircle: The eighth state uses a single motion sequence. The sequence cuts along the lower arc of the pattern approximately halfway around.

9) Check for Attachment: The ninth state occurs at the end of the Cut Upper Semicircle state. It combines two sensor measurements with a single motion sequence. The purpose of the state is to determine if the circle pattern has been successfully separated from the surrounding OTP. To determine this, we introduce an additional sensing step that deforms the OTP by moving the circle. First, we image a $p_{9,1} = 250 \times 250$ pixel window at a known offset from the center of the circle such that the still attached part of the circle is contained within the image window. Then, the gripper moves 8 mm to the right (that is, away from the left edge). Finally, we re-image the window. Then, we use the *matchTemplate* function of OpenCV to compute a difference metric for the two images [27] to detect separation.

If the edge has not moved, the state machine terminates, reporting success. If the edge has moved, we judge that the circle pattern has not been successfully separated, and so we attempt the last state, Final Cutting. This forms a loop, re-checking the attachment after the Final Cutting state. However, this loop is executed a maximum of two times for an increased success rate during repeated executions. If the circle is judged to attached after $p_{9,3} = 2$ Final Cutting attempts, the state machine terminates, declaring failure.

10) Final Cutting: The tenth state consists of a single motion sequence that consists of a multi-arm maneuver. The cutting tool moves $p_{10,1} = 2$ cm forward (that is, continuing along the arc it started with Cut Upper Semicircle). This was determined by a binary search between empirically determined bounds of 1.5 cm, below which scissor tool is unable to introduce sufficient tension in the gauze to be able to cut the attached end; and an upper bound of 3.5 cm, which pulls the gauze out of the OTP fixture clips. To avoid colliding with the gripper arm, the gripper arm moves $p_{10,2} = 1.5$ cm in the same direction, and $p_{10,3} = 1$ cm towards the cutting tool.

Trial	Length (mm)	Outcome	Retractions	Cut Failures	Time (s)	
					Total	Mean
1	21	Success	3	0	70	20.3
2	22	Success	3	0	70	20.3
3	27	Success	3	0	73	21.3
4	27	Success	4	1	94	20.5
5	24	Success	3	0	73	21.3
					76	20.8

TABLE I: Results for 3d-DVTP with linear tumor targets. We performed five trials, all of which succeeded in fully debriding the targets. Four trials required three retractions to complete, while one required four retractions and also experienced a cut failure. The average total time was 76 seconds, with a standard deviation of 10.2. The mean time of debridement per target was 20.8 seconds.

Trial	Targets	Failures		Time (s)	
		Detection	Cut	Total	Mean
1	5	0	0	128	23.2
2	5	0	0	127	23.0
3	5	0	0	125	22.6
4	5	0	0	128	23.2
5	5	0	0	128	23.2
6	5	0	0	127	23.0
7	5	1	1	103*	23.5
8	5	0	0	125	22.6
9	5	0	0	125	22.6
10	5	0	0	124	22.4
	50	1	1	—	22.3

TABLE II: Results for 3d-DVTP with spherical tumor targets 2 mm in diameter. Ten trials were performed, with five targets in each trial. In nine of the ten trials, all five targets were successfully debrided. In the remaining trial, the fourth target experienced a cut failure, where target was not entirely severed from the VTP. Subsequent to this, the fifth target failed to be detected. This detection failure caused the total time, marked above by *, to be lower than other trials. The total success rate was 48 out of 50 targets, or 96%. The average time per target was 25.3 seconds. The adjusted mean was 22.3 seconds.

VI. Experimental Evaluation

A. Debridement of 3D Viscoelastic Tissue Phantom (3d-DVTP)

Using the FSM from Section V-A, we performed the 3d-DVTP subtask with two kinds of tumor targets: linear and spherical.

1) Linear Tumor Targets: We used targets of lengths between 21 and 27 mm. We ran 5 trials with the targets in four different orientations. Four trials required three retractions to complete, while one required four retractions. The average total time was 76 seconds, with a standard deviation of 10.2. The mean time of debridement per target was 20.8 seconds.

2) Spherical Tumor Targets: We performed a randomization procedure to place spherical targets in the VTP. The debris was placed on the VTP using randomly-generated

Trial	Success	Score	Failed State	Transl. (mm)		Total Time
				x	y	
Demonstration		99.86		0.0	0.0	263
1	Success	99.81	—	26.4	-1.0	284
2	Failure	—	Notch	2.0	-0.5	130*
3	Failure	—	Notch	1.2	-3.0	120*
4	Success	94.52	—	4.5	-2.1	289
5	Failure	—	L.S.	2.0	-1.4	115*
6	Success	97.32	—	-1.2	-2.2	283
7	Success	99.12	—	4.0	-0.9	282
8	Failure	—	Notch	3.6	-0.9	131*
9	Failure	—-	U.S.	8.1	0.2	248*
10	Success	98.89	—	5.6	-0.4	279
11	Failure	—-	Notch	8.5	-1.8	129*
12	Success	99.87	—	5.6	-0.8	279
13	Success	100.00	—	6.6	0.4	284
14	Success	99.96	—	2.3	-1.6	285
15	Success	99.86	—	3.0	0.3	283
16	Success	98.96	—	9.3	-0.4	284
17	Success	98.39	—	8.5	-0.7	285
18	Success	98.94	—	10.5	-0.7	284
19	Success	98.85	—	9.3	0.5	284
20	Success	99.98	—	6.8	0.8	284
Mean	70%	98.89		6.5	1.0	284
Std. Dev.		1.47		5.6	0.8	2.5

TABLE III: Results for 2d-PCOTP. Twenty trials were performed, with a 70% success rate. The mean completion time for the successful trials (excluded times marked with an asterisk) was 284 seconds, less than the required limit of 300 seconds. The mean quality of successful trials was 99.89. For the Failed State column, "L.S." and "U.S" stand for the Lower and Upper Semicircle Cutting states, respectively. The average translation of the circle from its position in the demonstration was 6.5 mm in the x direction and 1.0 mm in the y direction. In FLS, "expert proficiency" is granted to surgical trainees when the pattern cutting is completed in 162 seconds with no errors [12].

coordinates. Using the visual segmenting described in Section IV-C, we uniformly sampled a rectangle containing the VTP contour and kept only samples falling inside the contour. We also rejected samples falling within 40 pixels of existing samples, so that the targets were not too close together. The coordinates were overlaid on the picture, and this was used to place the targets in the VTP.

We performed 10 trials with 5 spherical targets each. The results are shown in Table II. We measured the total runtime of the debridement, from which the mean per-target time was calculated.

In nine of the ten trials, all five targets were successfully debrided. In the remaining trial, the fourth target experienced a cut failure. Subsequent to this, the fifth target failed to be detected. The total success rate was 48 out of 50 targets, or 96%. The mean time of debridement per target was 22.3 seconds.

B. Pattern Cutting of Orthotropic Tissue Phantom (2d-PCOTP)

For 2d-PCOTP, we used the equipment from the FLS kit using one layer of gauze. The deformation of the gauze is characterized by the orthotropic nature of the material.

Using the FSM and parameter vector, the system performed 20 trials. The translation in the circle from its position during the demonstration, as detected by our ellipse-fitting algorithm, was up to 26.4 mm in the x direction (left to right), and up to 3 mm in the y direction, with an average of 6.5 mm and 1.0 mm, respectively.

The results are shown in Table III. Of the six trials that failed, four of these failed in the fourth state, notch cutting. One trial failed for each of the upper and lower semicircle cutting states due to the deformation of the material not matching the deformation experienced during the demonstration. The average execution time for the successful trials was 284 seconds, with a standard deviation of 2.5 seconds. The variation in time was due to differences in the execution of the final state. All of the trials completed in under 300 seconds. In FLS, "expert proficiency" is granted when the task is completed in 162 seconds with no errors [12].

We found the average quality, as computed by Eqn. (1), to be 99.89, with a standard deviation of 1.47. This is slightly higher than the quality of the demonstration, which was 99.86. The minimum quality of the autonomous system for a successful trial was 94.52.

VII. Conclusion and Future Work

Initial experiments suggest that thse subtasks can be reliably automated using LBO but performance times are at least twice as slow as expert human teleoperation. The next steps are to continue parameter tuning to further reduce execution time, extend the vision system to allow denser arrangements of tumor targets, develop analytic models of deformable tissue, and apply the LBO framework to other FLS subtasks, axillary dissection [20], and cardiothoracic vein harvesting [34].

Acknowledgments

We thank our collaborators, in particular Allison Okamura, Greg Hager, Blake Hannaford, and Jacob Rosen. We thank Intuitive Surgical, and in particular Simon DiMao, for making the DVRK possible. We also thank the DVRK community, including Howie Choset, Anton Deguet, James Drake, Greg Fisher, Peter Kazanzides, Tim Salcudean, Nabil Simaan, and Russ Taylor. We also thank Aliakbar Toghyan, Barbara Gao, Raghid Mardini, and Sylvia Herbert for their assistance on this project. This work is supported in part by a seed grant from the UC Berkeley Center for Information Technology in the Interest of Science (CITRIS), by the U.S. National Science Foundation under Award IIS-1227536: Multilateral Manipulation by Human-Robot Collaborative Systems, by AFOSR-YIP Award #FA9550-12-1-0345, and by Darpa Young Faculty Award #D13AP00046.

References

[1] R. Alterovitz and K. Goldberg, *Motion Planning in Medicine: Optimization and Simulation Algorithms for Image-guided Procedures*. Springer, 2008.

[2] B. D. Argall, S. Chernova, M. Veloso, and B. Browning, "A Survey of Robot Learning from Demonstration," *Robotics and Autonomous Systems*, vol. 57, no. 5, pp. 469–483, 2009.

[3] C. E. Attinger, E. Bulan, and P. A. Blume, "Surgical Debridement: The Key to Successful Wound Healing and Reconstruction," *Clinics in podiatric medicine and surgery*, vol. 17, no. 4, p. 599, 2000.

[4] G. Ballantyne and F. Moll, "The da Vinci Telerobotic Surgical System: The Virtual Operative Field and Telepresence Surgery," *Surgical Clinics of North America*, vol. 83, no. 6, pp. 1293–1304, 2003.

[5] R. A. Beasley, "Medical Robots: Current Systems and Research Directions," *Journal of Robotics*, vol. 2012, 2012.

[6] S. Billings, N. Deshmukh, H. Kang, R. Taylor, and E. Boctor, "System for Robot-Assisted Real-Time Laparoscopic Ultrasound Elastography," in *SPIE Medical Imaging*, 2012.

[7] G. Bradski and A. Kaehler, *Learning OpenCV: Computer Vision with the OpenCV Library*. O'Reilly, 2008.

[8] S. Calinon, "Robot Programming by Demonstration," in *Springer handbook of robotics*, 2008, pp. 1371–1394.

[9] N. Chentanez, R. Alterovitz, D. Ritchie, L. Cho, K. Hauser, K. Goldberg, J. R. Shewchuk, and J. F. O'Brien, "Interactive Simulation of Surgical Needle Insertion and Steering," *ACM Transactions on Graphics*, vol. 28, no. 3, 2009.

[10] S. A. Darzi and Y. Munz, "The Impact of Minimally Invasive Surgical Techniques," in *Annu Rev Med.*, vol. 55, 2004, pp. 223–237.

[11] K. Dixon, "Inferring User Intent for Learning by Observation," Ph.D. dissertation, Carnegie Mellon University, 2004.

[12] G. Dulan, R. V. Rege, D. C. Hogg, K. M. Gilberg-Fisher, N. A. Arain, S. T. Tesfay, and D. J. Scott, "Developing a Comprehensive, Proficiency-based Training Program for Robotic Surgery," *Surgery*, vol. 152, no. 3, pp. 477–488, 2012.

[13] M. Gienger, M. Muhlig, and J. J. Steil, "Imitating Object Movement Skills with Robots: A Task-Level Approach Exploiting Generalization and Invariance," in *IEEE/RSJ Int. Conf. on Intelligent Robots and Systems (IROS)*, 2010, pp. 1262–1269.

[14] M. Granick, J. Boykin, R. Gamelli, G. Schultz, and M. Tenenhaus, "Toward a Common Language: Surgical Wound Bed Preparation and Debridement," *Wound repair and regeneration*, vol. 14, no. s1, pp. 1–10, 2006.

[15] B. Hannaford, J. Rosen, D. C. Friedman, H. King, P. Roan, L. Cheng, D. Glozman, J. Ma, S. Kosari, and L. White, "Raven-II: An Open Platform for Surgical Robotics Research," *IEEE Transactions on Biomedical Engineering*, vol. 60, pp. 954–959, Apr. 2013.

[16] Intuitive Surgical, "da Vinci Research Kit," 2014. [Online]. Available: http://research.intusurg.com/dvRK

[17] P. Kazanzides, Z. Chen, A. Deguet, G. Fischer, R. Taylor, and S. DiMaio, "An Open-Source Research Kit for the da Vinci Surgical System," in *Proc. IEEE Int. Conf. Robotics and Automation (ICRA)*, 2014.

[18] B. Kehoe, G. Kahn, J. Mahler, J. Kim, A. Lee, A. Lee, K. Nakagawa, S. Patil, W. Boyd, P. Abbeel, and K. Goldberg, "Autonomous Multilateral Debridement with the Raven Surgical Robot," in *Proc. IEEE Int. Conf. Robotics and Automation (ICRA)*, 2014.

[19] G. Konidaris, S. Kuindersma, R. Grupen, and A. Barto, "Robot Learning from Demonstration by Constructing Skill Trees," *Int. Journal of Robotics Research*, vol. 31, no. 3, pp. 360–375, 2011.

[20] S. M. Lim, C. K. Kum, and F. L. Lam, "Nerve-sparing Axillary Dissection using the da Vinci Surgical System," *World Journal of Surgery*, vol. 29, no. 10, pp. 1352–1355, 2005.

[21] H. C. Lin, I. Shafran, D. Yuh, and G. D. Hager, "Towards Automatic Skill Evaluation: Detection and Segmentation of Robot-assisted Surgical Motions," *Computer Aided Surgery*, vol. 11, no. 5, pp. 220–230, 2006.

[22] H. Mayer, I. Nagy, D. Burschka, A. Knoll, E. Braun, R. Lange, and R. Bauernschmitt, "Automation of Manual Tasks for Minimally Invasive Surgery," in *Int. Conf. on Autonomic and Autonomous Systems*, 2008, pp. 260–265.

[23] O. Mohareri, P. Black, and S. E. Salcudean, "da Vinci Auxiliary Arm as a Robotic Surgical Assistant for Semi-Autonomous Ultrasound Guidance during Robot-Assisted Laparoscopic Surgery," in *Hamlyn Symposium on Medical Robotics (HSMR)*, 2014.

[24] G. Moustris, S. Hiridis, K. Deliparaschos, and K. Konstantinidis, "Evolution of Autonomous and Semi-Autonomous Robotic Surgical Systems: A Review of the Literature," *Int. Journal of Medical Robotics and Computer Assisted Surgery*, vol. 7, no. 4, pp. 375–392, 2011.

[25] S. Niekum, S. Osentoski, G. Konidaris, S. Chitta, B. Marthi, and A. G. Barto, "Learning Grounded Finite-State Representations from Unstructured Demonstrations," *Int. Journal of Robotics Research*, vol. 34, no. 2, pp. 131–157, 2015.

[26] H.-W. Nienhuys and A. F. van der Stappen, "A Surgery Simulation supporting Cuts and Finite Element Deformation," in *Medical Image Computing and Computer-Assisted Intervention–MICCAI 2001*. Springer, 2001, pp. 145–152.

[27] OpenCV, "Template matching." [Online]. Available: http://docs.opencv.org/doc/tutorials/imgproc/histograms/template_matching/template_matching.html

[28] T. Osa, N. Sugita, and M. Mamoru, "Online Trajectory Planning in Dynamic Environments for Surgical Task Automation," in *Robotics: Science and Systems (RSS)*, 2014.

[29] N. Padoy and G. Hager, "Human-Machine Collaborative Surgery using Learned Models," in *Proc. IEEE Int. Conf. Robotics and Automation (ICRA)*, 2011, pp. 5285–5292.

[30] C. E. Reiley and G. D. Hager, "Task versus Subtask Surgical Skill Evaluation of Robotic Minimally Invasive Surgery," in *Medical Image Computing and Computer-Assisted Intervention (MICCAI)*, 2009, pp. 435–442.

[31] C. E. Reiley, E. Plaku, and G. D. Hager, "Motion generation of robotic surgical tasks: Learning from expert demonstrations," in *Engineering in Medicine and Biology Society (EMBC), 2010 Annual International Conference of the IEEE*. IEEE, 2010, pp. 967–970.

[32] E. Ritter and D. Scott, "Design of a Proficiency-based Skills Training Curriculum for the Fundamentals of Laparoscopic Surgery," *Surgical Innovation*, vol. 14, no. 2, pp. 107–112, 2007.

[33] J. Schulman, A. Gupta, S. Venkatesan, M. Tayson-Frederick, and P. Abbeel, "A Case Study of Trajectory Transfer through Non-Rigid Registration for a Simplified Suturing Scenario," in *IEEE/RSJ Int. Conf. on Intelligent Robots and Systems (IROS)*, 2013, pp. 4111–4117.

[34] K. D. Stahl, W. D. Boyd, T. A. Vassiliades, and H. L. Karamanoukian, "Hybrid Robotic Coronary Artery Surgery and Angioplasty in Multivessel Coronary Artery Disease," *The Annals of thoracic surgery*, vol. 74, no. 4, pp. 1358–1362, 2002.

[35] R. Taylor, A. Menciassi, G. Fichtinger, and P. Dario, "Medical Robotics and Computer-Integrated Surgery," *Springer Handbook of Robotics*, pp. 1199–1222, 2008.

[36] J. Van Den Berg, S. Miller, D. Duckworth, H. Hu, A. Wan, X. Fu, K. Goldberg, and P. Abbeel, "Superhuman Performance of Surgical Tasks by Robots using Iterative Learning from Human-Guided Demonstrations," in *Proc. IEEE Int. Conf. Robotics and Automation (ICRA)*, 2010, pp. 2074–2081.

[37] B. Varadarajan, C. Reiley, H. Lin, S. Khudanpur, and G. Hager, "Data-derived Models for Segmentation with Application to Surgical Assessment and Training," in *Medical Image Computing and Computer-Assisted Intervention (MICCAI)*, 2009, pp. 426–434.

[38] R. Veldkamp, E. Kuhry, W. Hop, J. Jeekel, G. Kazemier, H. J. Bonjer, E. Haglind, L. Pahlman, M. A. Cuesta, S. Msika, *et al.*, "Laparoscopic surgery versus open surgery for colon cancer: short-term outcomes of a randomised trial," *Lancet Oncol*, vol. 6, no. 7, pp. 477–484, 2005.

[39] A. Wolf and M. Shoham, "Medical Automation and Robotics," in *Springer Handbook of Automation*, 2009, pp. 1397–1407.

[40] H. Zhang, S. Payandeh, and J. Dill, "On Cutting and Dissection of Virtual Deformable Objects," in *Proc. IEEE Int. Conf. Robotics and Automation (ICRA)*, 2004, pp. 3908–3913.